Journal of the Mechanics and Physics of Solids 124 (2019) 350–365

Contents lists available at ScienceDirect

Journal of the Mechanics and Physics of Solids

journal homepage: www.elsevier.com/locate/jmps

Fracture mechanics of nacre-like materials using discrete-element models: Effects of microstructure, interfaces and randomness

Najmul Abid, J William Pro, Francois Barthelat*

Department of Mechanical Engineering, McGill University, 817 Sherbrooke Street West, Montreal, QC H3A 2K6, Canada

ARTICLE INFO

Article history:
Received 24 April 2018
Revised 21 July 2018
Accepted 15 October 2018
Available online 19 October 2018

Keywords:
Discrete element modeling
Staggered composites
Nacre, Bone
Toughness
Fracture mechanics
Random microstructures

ABSTRACT

Biological materials such as nacre, bone and spider silk boast unusual combinations of stiffness, strength and toughness. Behind this performance is the staggered arrangement of stiff and elongated inclusions embedded in a softer and more deformable matrix. In this study, we use the discrete element method (DEM) to simulate large fracture models of staggered composites (up to 450,000 tablets). The models explore the combined effects of tablet arrangement, interface properties and statistical variations on fracture mechanics: crack deflection, crack bridging, volumetric process zones of different size and shapes, transient and steady-state crack propagation regimes, full crack resistance curves. We find that moderate statistical variations in the microstructure increases toughness because the crack gets pinned into tougher regions. However, higher statistical variations generate very weak regions which can be activated far from the main crack, leading to discontinuous cohesive zones, sparse process zones, and an overall decrease in toughness. These results suggest an important rule for the design of nacre-like materials: microstructural randomness should be minimized to achieve the highest combinations of properties.

© 2018 Published by Elsevier Ltd.

1. Introduction

Structural biological materials such as seashells and bones are made of relatively weak small-scale components, but they are assembled in architectures that lead to remarkable combinations of mechanical properties. In some cases, the amplification of their mechanical performance is unmatched by any synthetic material (Barthelat and Rabiei, 2011; Munch et al., 2008). This remarkable amplification can be attributed to the staggered architecture, where elongated mineral inclusions are aligned in the direction of loading in a “brick-and-mortar” arrangement, and with interfaces composed of soft bio-polymeric layers. The most common example of a staggered structure is nacre, which consists of aligned aragonite tablets (~95 % vol) bonded together with a very thin organic layer (~5 % vol) (Fig. 1a and b). Another example of a staggered structure is bone, which is composed of osteons separated by weaker interfaces at the millimeter scale . At smaller scales, collagen fibrils consist of a staggered arrangement of tropocollagen molecules (Fratzl et al., 1998) and elongated nano-minerals that can glide on one another under stress (Gupta et al., 2006). Other examples of staggered arrangement include tooth enamel (Nishikawa, 1992) and spider silk (Keten et al., 2010). Interestingly, the staggered architecture has been identified as an optimal arrangement to combine stiffness, strength and energy absorption in uniaxial tension (Barthelat and Mirkhalaf, 2013).

* Corresponding author.
E-mail address: francois.barthelat@mcgill.ca (F. Barthelat).

https://doi.org/10.1016/j.jmps.2018.10.012
0022-5096/© 2018 Published by Elsevier Ltd.

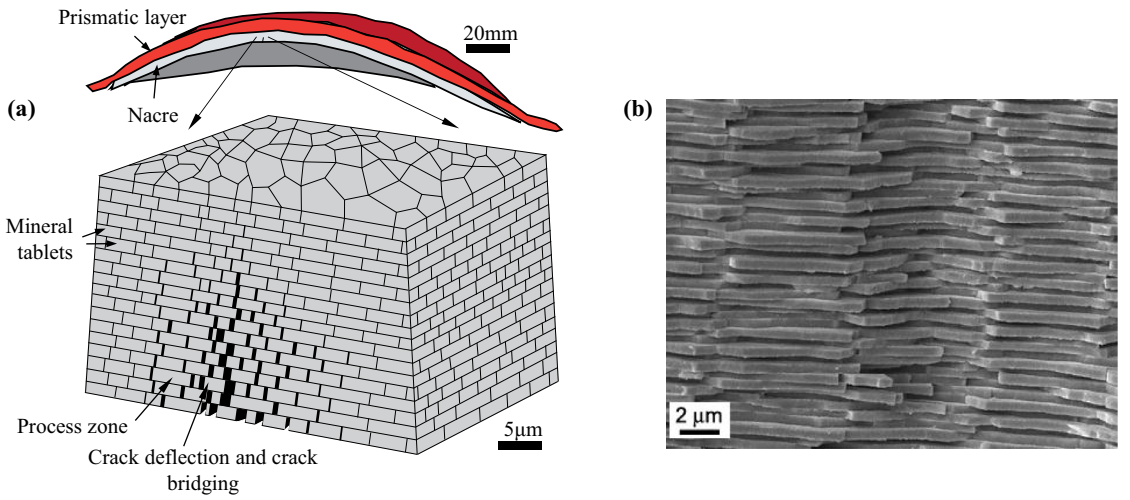

Fig. 1. (a) Schematic of a mollusk shells showing the microstructure of nacre and some of its main mechanisms of fracture. (b) Fracture surface of nacre showing statistical variations within the size and arrangement of the tablets (adapted from Barthelat, Tang (Barthelat et al., 2007)).

In particular, the best combinations of properties are reached when there is a large contrast of strength between the tablets and the interfaces (Barthelat, 2014; Barthelat and Mirkhalaf, 2013; Begley et al., 2012; Guo and Gao, 2006; Rabiei et al., 2010; Wegst et al., 2015), and when the deformability of the interfaces in shear is very high to allow for large tablet sliding distances (Barthelat and Rabiei, 2011; Barthelat et al., 2016). In recent years, several synthetic materials inspired by nacre were proposed. These materials were fabricated using a variety of methods including self-assembly (Bonderer et al., 2008), freeze casting (Deville et al., 2006), filtration (Liu et al., 2011), sedimentation (Behr et al., 2015), doctor blading (Mirkhalaf and Barthelat, 2016) or directed mineralization (Mao et al., 2016). In these “nacre-like” microstructures, the precise control of the arrangement of microscopic tablets over large volumes is difficult and still presents formidable challenges. As a result of limitation in the fabrication methods, statistical variations and randomness in the microstructure of synthetic nacre are still much greater than what is observed in natural nacre (Bai et al., 2016).

The impact of these significant statistical variations on the fracture toughness of nacre-like materials is still not clear. A recent study by Pro, Lim (Pro et al., 2015) showed that fracture toughness decreases substantially with statistical variations. However, this study did not consider strain hardening and only simulated running bond-type nacre (50% overlap) and only considered initiation toughness. Other studies suggest that small random variations in the microstructure can increase toughness (Barthelat et al., 2007). For example Hossain, Hsueh (Hossain et al., 2014) simulated crack propagation in brittle materials with tough and weak periodic layers and showed that the resistance to crack growth could increase or decrease depending on the location of the crack tip. Needleman and Tvergaard (Needleman and Tvergaard, 1991) and Srivastava, Ponson (Srivastava et al., 2014) have examined the effect of uniform and non-uniform distributions of voids and inclusions in front of a crack propagating in a ductile material. They showed that non-uniform distributions results in the crack being pinned in tougher regions, leading to higher toughness. The exact effects of statistics on the fracture toughness of staggered composites therefore remains an open question, with important implications in the design of bio-inspired materials.

A significant challenge in modeling the fracture of composites at large scales is to manage the high computational cost associated. There are multiple toughening mechanisms that act together during crack propagation at multiple length scales (Mayer, 2005), some of them involving large volumes of material. The size of the process zone can be up to two orders of magnitude larger than the base constituents themselves (Rabiei et al., 2010), a mechanism similar to that found in ductile metals (Tvergaard and Hutchinson, 1992) and toughened rubbers (Evans et al., 1986). Several numerical simulations have been presented in the past for nacre-like materials. With these numerical approaches, large volumes of material with nonlinear response, containing cracks and subjected to complex stress states can be captured to a level of complexity which analytical models fail to capture (Askarinejad and Rahbar, 2015; Barthelat et al., 2007; Katti and Katti, 2001; Pro et al., 2015). However, the majority of numerical models are based on bulk finite elements coupled with cohesive elements, an approach which can be computationally expensive (Anup, 2015; Barthelat et al., 2007; Katti and Katti, 2001; Mirkhalaf and Barthelat, 2016; Niebel et al., 2016). Only a few hundred tablets can be modeled at most (Barthelat et al., 2007), which is not sufficient to capture the effect of statistical variations on the overall performance. Discrete element modeling (DEM) is an alternative numerical method that has been used recently to model deformation and fracture in staggered composites at a fraction of the computational cost of finite elements (Abid et al., 2018; Chandler and Cheng, 2018; Pro et al., 2015; Pro et al., 2015). In a previous article (Abid et al., 2018), we have used DEM to explore the mechanical response of large representative volume elements continuing statistical microstructures. This study showed how seemingly small statistical variations precipitate strain localization and decrease energy absorption by a large amount. We also found that the detrimental effects of statistical microstructures can be partially offset by large deformations and strain hardening at the interfaces

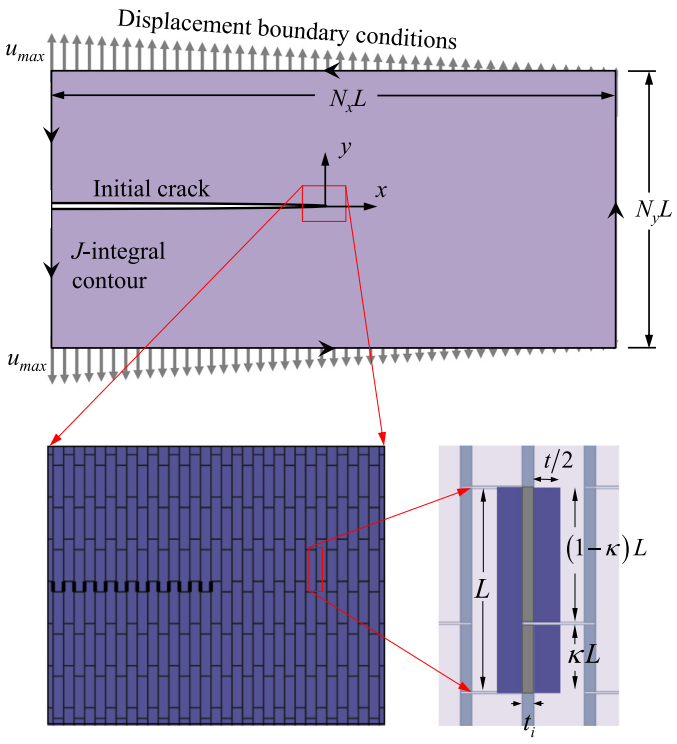

Fig. 2. Overview of the fracture DEM model showing overall model with dimensions, boundary conditions and J-integral contour, and close-up views showing tablet arrangement and structural parameters on a unit cell.

(Abid et al., 2018), which are features typically observed in the weak structural interfaces within biological materials (Barthelat et al., 2016). In this follow up study we used the DEM approach to capture crack propagation in nacre-like architectures. The objectives were first to capture the salient mechanisms of fracture in nacre-like composites: crack deflection at the interfaces, crack bridging, large scale inelastic deformations ahead and behind advancing cracks, process zone toughening, R-curve behavior. A second objective was to systematically explore the effects of microstructure (including statistics) and interface properties on the fracture of nacre-like materials.

2. Fracture model setup and validation

Fig. 2 shows a schematic of the setup for the fracture model. The model generation and DEM formulation is similar to our previous work on nacre-like materials subjected to uniaxial tension (Abid et al., 2018), but for this study on fracture all the models contained a deep notch. Tablets of length L and thickness t are arranged in a staggered fashion and are bonded by an interface with thickness $ti < t$. The tablets overlap by a length κL with $0 < \kappa \leq 0.5$ (stagger is generated by shifting every odd row of tablet by a distance κL). The resulting nacre-like microstructure can be described by three independent dimensionless parameters: tablets aspect ratio $\rho = \frac{L}{t}$, overlap ratio κ and tablet volume concentration $\phi = \frac{t}{t+t_i}$ $(0 < \phi < 1)$. The arrangement is repeated in the x and y directions to form a two dimensional periodic tiling made of N_x by N_y tablets (typical dimensions were $N_x = 1{,}500$, $N_y = 300$ for a total of 450,000 tablets).

The tablets were assumed to be rigid compared to the interfaces, an assumption which is acceptable for materials like nacre or bone where the contrast of stiffness and strength between matrix and inclusion is in the order of 100–1000 (Barthelat, 2015; Pro et al., 2015). We also neglected the rotation of individual tablets and their displacement along the x direction (direction of crack propagation, Fig. 2), which saved significant computational time. This assumption is based on experimental observations on nacre where the shearing of the interface due to tablet sliding dominates, while the contribution of the other degrees of freedom appears to be negligible in comparison (Barthelat et al., 2007). We have validated this assumption by running an additional set of simulations that included all three degrees of freedom and comparing the steady state toughness to the uniaxial model. We observed less than a 2.1% difference of in predicted toughness between the models, indicating that neglecting rotations and displacements along the x direction is acceptable. The effect of the multiaxial stress state ahead of the crack is of higher order and does not alter the computed fracture properties significantly in this model, in consistence with recent stress calculations on nacre-like models (Pro et al., 2015). Combining these assumptions implies that the distribution of shear stress at the interfaces is uniform, and that there are no peeling stresses. As a result, the interaction between individual tablets can be modeled by a single nonlinear spring element. The mechanical

response of the interfaces is governed by a nonlinear shear stress-strain law and by the length of the overlapping interface between two adjacent tablets. The interfaces depicted on Fig. 2 are perfectly flat, whereas, in natural nacre interfaces are wavy (Barthelat et al., 2007). However, since the DEM approach idealizes each interface as a nonlinear element, the exact morphology of the interface does not need to be captured. The added shear resistance generated by tablets waviness or by nano-asperities can simply be taken into account by increasing the strength and the hardening rate of the nonlinear spring element using to model the response of the interface. The global response of large assemblies of tablets was computed using a DEM scheme on Matlab (Mathews and Fink, 2004), with the classical Newton-Raphson method (Press et al., 2007) and with continuous stiffness and Jacobian updates to solve the nonlinear system. Details on the DEM code and model validations can be found in our previous report (Abid et al., 2018). A deep notch was created across the direction of the tablets by simply removing the discrete (cohesive) elements along the crack line, so that the initial tip of the notch was centered on the model (Fig. 2). A linear spatial distribution of displacement boundary conditions was applied on the upper and lower boundaries of the models (Fig. 2). The upper displacement followed the linear distribution:

$$u(x) = u_{\max}\left(\frac{1}{2} - \frac{x}{N_x L}\right) \tag{1}$$

where u_{max} is the maximum displacement (at $x = -N_x L/2$). The lower boundary was subjected to the equivalent symmetric distribution. This particular type of non-uniform distribution of displacement boundary conditions promotes stable crack propagation in the system (Pro et al., 2015; Tada et al., 1973) and is compliant to that of the Hill-Mandel condition (Nguyen et al., 2012). Left and right boundaries ($x = \pm N_x L/2$) were free surfaces. During the simulation u_{max} was progressively increased and the boundary condition were increased following Eq. (1) to propagate a mode I crack through the model. Stable crack propagation could be achieved in all simulations, as verified by numerical convergence for small incremental crack advances to a new stable equilibrium state as the loading was ramped. At each loading step, the length of the crack was measured and the *J*-integral (Rice, 1968) was computed along an integration contour taken as the outer boundary of the model (Fig. 2) using:

$$J = \int_{\Gamma}\left(W n_1 - t_i \frac{\partial u_i}{\partial x_1}\right) d\Gamma \tag{2}$$

where W is the strain energy density, n_1 is the 1st component of the normal vector to the contour, t_i is the traction vector, u_i is the displacement vector and Γ is the contour path. Because the top and the bottom edges of the integration contour were taken through the tablets and the integration contour of the other two edges (left and right) were taken through the interfaces, the *J*-integral (Eq. 2) simplified to only the strain energy density of the interfaces and the net reaction forces and displacements of the tablets on which the boundary conditions were applied. The *J*-integral may become path dependent if the material system is discrete, or when significant unloading occurs (Kolednik et al., 2014; Rice and Rosengren, 1968; Simha et al., 2008). However, several reports have shown that if the plastic unloading is relatively small and the integration contour is taken far away from the crack tip, the *J*-integral can be path independent (Kolednik et al., 2014; Simha et al., 2008). In our models we ensured that the *J*-integral was path independent by making the model size very large (in this case the model was 1500 by 300 tablets) and by taking the *J*-integral contour near the outer edges (Fig. 2). For a given model size, we also verified that different contours led to the same *J* value (not shown here). As discussed below, our model and the *J*-integral calculation setup could recover analytical solutions where fracture is dominated by tablet bridging. The main outcome for each simulation was the crack resistance curve for a particular set of staggered microstructure and cohesive law. We explored three types of staggered microstructures: running bond, columnar and sheet nacre. In the running bond microstructure, the tablets overlap by half of their length ($\kappa = 1/2$). In columnar nacre the tablets partially overlapped with $0 < \kappa < 0.5$. Finally in sheet nacre, each row of tablets was randomly shifted by a distance rL, where r is a uniformly distributed random number between 0 and 1.

3. Toughness and cohesive length using triangular interface laws

Fig. 3 shows a close up view of a simulation with columnar nacre ($\kappa = 0.25$, $\rho = 4$, $N_x = 1{,}000$, $N_y = 200$). In this model we used a triangular shear stress strain law shown in Fig. 3a defined by an initial elastic region with shear modulus G up to a shear stress τ_0, followed by a post-peak softening region up to complete failure of the interface at $\gamma = \gamma_u$. The shear stress-strain curve was converted into a cohesive law by computing the sliding distance $\Delta u = \gamma t_i$, and the toughness of the interface is given by:

$$J_i = t_i \int_0^{\gamma_u} \tau \, d\gamma \tag{3}$$

The evolution of the crack as the applied displacement was increased is shown in Fig. 3b. Initially, all the interfaces deformed elastically until the highest stressed interfaces just ahead of the crack tip reached the yield strength, and immediately entered the softening region of the interface law (these interfaces are highlighted in red on Fig. 3b). As the applied displacement increased further, more interfaces softened, creating a narrow process zone in front of the crack tip (snapshot 2). Once the interface just ahead of the notch reached the ultimate strain γ_u, its cohesive traction vanished, and the crack propagated by a distance t (thickness of one tablet). Increasing the applied displacements resulted in stable crack propagation across the model (snapshot 3 in Fig. 3b). We defined the steady state cohesive length λ as the strip of interfaces that

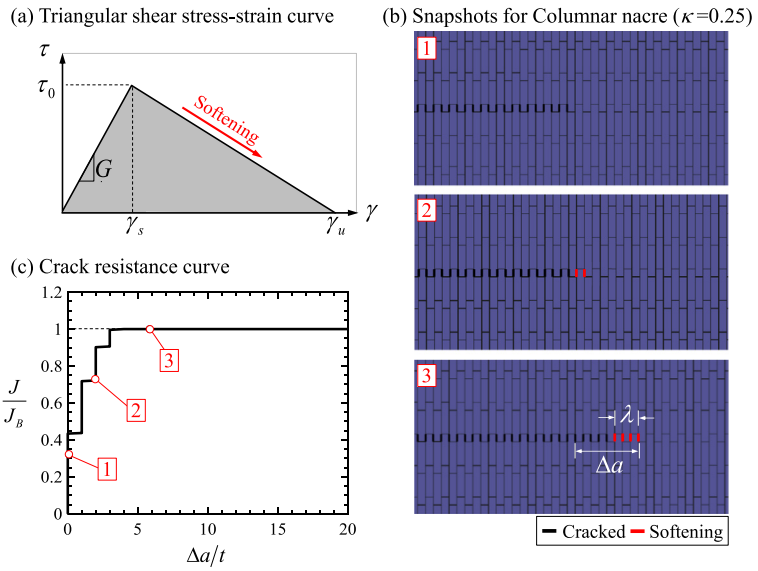

Fig. 3. (a) Example of triangular interface law (here $\gamma_u/\gamma_s = 4$); (b) Sequence of deformation and crack propagation (these magnified snapshots only represent about 3% of the full model). (c) Corresponding crack resistance curve.

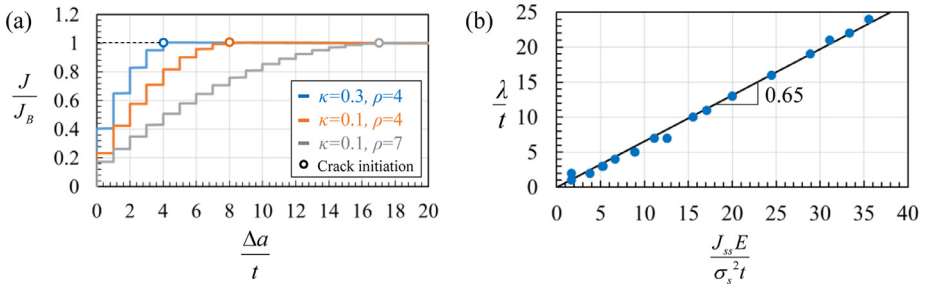

Fig. 4. (a) Crack resistance curves for three models with triangular interface law with different combinations of κ and ρ. (b) Comparison of the dimensionless cohesive length, λ/t, with $J_{ss}E/\sigma_s^2 t$ for the triangular interface law.

has reached the softening region in the steady state crack propagation regime. For example on Fig. 3, the cohesive length is $\lambda = 3t$. Fig. 3c shows the computed J-integral as a function of crack propagation (crack resistance curve). J progressively increases as the cohesive zone develops and reaches a steady state value when the crack propagates. For comparison we use the simple tablet bridging model (Barthelat and Rabiei, 2011):

$$J_B = \kappa \rho J_i \tag{4}$$

where J_i is the toughness of the interface defined above (Eq. 3). On Fig. 3c the toughness is normalized using J/J_B as a function of dimensionless crack extension $\Delta a/t$. In the steady-state regime, the DEM model properly recovers the analytical solution for all increments in crack advance (which is the bridging model (Barthelat and Rabiei, 2011)) with $J_{ss} = J_B$ which serves as a benchmark. We note that a minimum model size is required to achieve this result. For this particular model, N_x and N_y were progressively increased until the crack resistance curve was model size independent. For all of the results presented in this report we verified that model size independence was achieved (typically convergence required a model size of about $N_x = 1{,}500$ and $N_y = 300$ for a total of 450,000 tablets). We also ensured that the J values were path independent by computing about different contours. We also note that in the particular case of a triangular cohesive law, the steady state cohesive length λ can also be obtained by measuring Δa at the onset of stable crack propagation (on the example of Fig. 3, $\Delta a = 3t$). The DEM fracture model therefore captures the main features of fracture of nacre-like materials when a triangular interface law is used.

To further explore the effect of the key parameters on bridging toughness using triangular interface laws, we ran a large number of columnar models with various combinations of J_i, κ and ρ. Fig. 4a shows three examples crack resistance curves where κ and ρ were varied. As expected, all models recovered the theoretical solution $J_{ss} = J_B$. However, different combinations of parameters lead to different transient regimes and different steady state cohesive lengths. The relationship between the cohesive length λ and the applied energy release rate has been well documented for a variety of elementary

cohesive laws (Barenblatt, 1959; Dugdale, 1960; Hillerborg et al., 1976; Rice, 1979) and all indicate the direct scaling:

$$\lambda \sim \frac{J_{ss}E}{{\sigma_s}^2} \tag{5}$$

where J_{SS} is the steady state toughness, E is the Young's modulus and σ_s the tensile strength. For a staggered composite with rigid tablets the modulus and strength can be obtained with (Abid et al., 2018):

$$E = \frac{\phi^2}{1-\phi^2}\kappa(1-\kappa)\rho^2 G \tag{6}$$

and

$$\sigma_s = \phi\kappa\rho\tau_s \tag{7}$$

For the case of a triangular interface law the steady state toughness is:

$$J_{ss} = \kappa\rho J_i \tag{8}$$

Fig. 4b shows the normalized cohesive length λ/t as a function of $\frac{J_{ss}E}{{\sigma_s}^2 t}$ for various combinations of J_i, κ and ρ. We verified that the relationship is linear, with a slope of 0.65. For comparison, Lawn (Lawn, 1993) reported a slope of 0.392 for isotropic brittle materials. This value is in the same order but lower, because of the different nature of the materials (Lawn (Lawn, 1993) considered only homogeneous, isotropic brittle materials). When bridging is the only fracture mechanism, our nacre-like DEM models therefore recover the theoretical fracture toughness as well as the fundamental scaling laws for the cohesive length. In the next section we enrich the interface law and explore the effect on toughness and increasing process zone size.

4. Toughening from wide process zones: models with trapezoidal interface law

We now enrich the simple triangular interface law with a plateau region of constant shear stress to form a trapezoidal interface law. In this region, the plastic shear strain is defined as $\gamma^{(p)} = \gamma - \tau/G$, and softening starts at a plastic shear strain $\gamma^{(p)} = \gamma_s^{(p)}$. This type of interface constitutive law is typically used for modeling deformable engineering adhesives (Chalkley and Chiu, 1993) and bio-polymers (Smith et al., 1999), including the interfaces in nacre-like materials (Abid et al., 2018; Barthelat et al., 2007; Pro et al., 2015). The slope in the intermediate regime can be easily modified to capture strain hardening in the interfaces (Fig. 5a), where $\tau = \tau_y + H\gamma^{(p)}$ with $H > 0$. For simplicity, we assumed that any unloading in the interfaces from a strain $0 < \gamma < \gamma_u$ occurs along a segment of slope G, which allows for residual plastic strain in the interfaces. We also use the terms "yield point", "hardening" and "ductile" which are typically associated with the mechanics of metals, even if the materials in natural or bio-inspired composites may not be metallic. In the DEM fracture models, switching from a triangular to trapezoidal interface law produced a wider process zone, with inelastic deformation spreading away from the crack line. The material "yields" in the region of high stresses at the crack tip – a mechanism similar to ductile metals (Tvergaard and Hutchinson, 1992) and toughened rubbers (Evans et al., 1986). Fig. 5 shows an example of a 450,000 tablet DEM fracture model that uses a trapezoid interface law with strain hardening ($H/G = 0.05$, Fig. 5a). In this typical example, when the applied displacements were increased a nonlinear region appeared and grew in size ahead of the crack tip (shown as yellow interfaces on Fig. 5b). Near the crack tip, most interfaces yielded. Further from the crack tip (but still within the process zone), yielding only occurred in the smaller overlapping interfaces. As crack propagation commenced the tip entered the nonlinear region, shifting the regions of high stress and the inelastic region, and leaving a wake of inelastically deformed material (shown as white interfaces on Fig. 5b). The crack resistance curve for this model is shown in Fig. 5c. In this example, the steady-state toughness was reached when $\Delta a = 29t$. The steady state toughness was in general much greater than the toughness produced by bridging only, an indication of the powerful toughening effect of the inelastic region. Crack propagating through this microstructure involves the inelastic loading and unloading of a large volume of material, which consumes a large amount of mechanical energy. These mechanisms duplicate experimental observations on biological columnar nacre, the "stress whitening" regions corresponding to regions where tablet sliding take place (Fig. 5d and e). These observations are also qualitatively consistent with the salient features of the theoretical fracture model of Barthelat and Rabiei (Barthelat and Rabiei, 2011). However, there are major differences in the two models regarding process zone shape, unsteady process zone, and distribution of damage and residual strain in the wake of the crack. In previous analytical models these parameters were estimated and served as input. In the present DEM models, these quantities are a natural outcome of the simulations.

The type of cohesive law used for the interfaces has profound impact on the size of the inelastic region and on the crack resistance curve. Fig. 6 shows the results of three simulations obtained with three different cohesive law. In the first case (Fig. 6a) a triangular law was used which produces a steady state toughness $J_{ss} = J_B$ and no inelastic process zone. When the interface law is enriched into a trapezoidal law a wide inelastic zone (width = $15t$) appears (Fig. 6b), but its contribution to toughness remains modest with only a 5% increase from the triangular case. The addition of hardening ($H/G = 0.05$) leads to a wider process zone (width = $27t$) which is also denser in inelastic deformations (Fig. 6b). These effects lead to a pronounced improvement in toughness (50%) with a longer transient regime thought the hardening was modest ($H/G = 0.05$). We ran a series of models to explore the correlations between inelastic zone size, cohesive length and

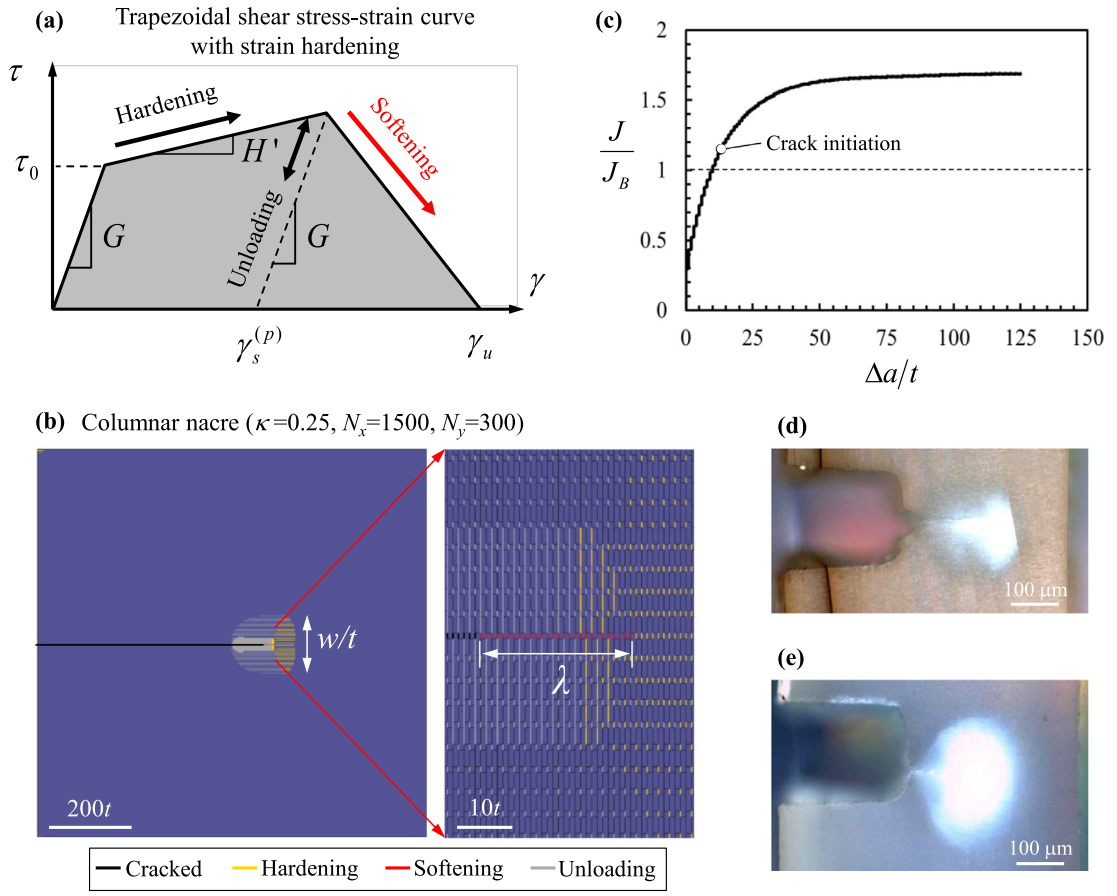

Fig. 5. (a) Trapezoidal interface law with strain hardening where $\tau_y/G = 0.09$, $\gamma_s/\gamma_y = 10$, $\gamma_u/\gamma_s = 6$ and $H/G = 0.05$. (b) Snapshot showing crack propagation and the associated volumetric process zone (here $w = 27t$ and $\lambda = 29t$) (c) Associated crack resistance curve. (d) Experimental observations of the process zone found in Top shell and in (e) red abalone (adapted from Rabiei, Bekah (Rabiei et al., 2010)).

toughness for different cohesive laws. Fig. 7a shows the result of ten simulations with different combinations of plateau length (γ_s/γ_y) and hardening slope. Toughness increased moderately with a trapezoidal cohesive law with $H = 0$, but it increased more significantly when hardening $H > 0$ was used at the interface. This result illustrates that strain hardening is a key contributor to fracture toughness amplification in both synthetic and natural systems. Hardening can be generated by a soft adhesive or matrix between the tablets, or by geometric hardening and progressive interlocking using dovetail-like tablets (Barthelat, 2010; Barthelat and Espinosa, 2007). For all calculations we performed, high toughness correlated with a large process zone.

The evolution of the cohesive length however appears to be more complex than for the cases of triangular cohesive law only. Fig. 7b shows the dimensionless cohesive length, λ / t as a function of $\frac{J_{SS}E}{\sigma_s^2 t}$ for a trapezoidal interface law. The results did not reveal a direct scaling, but rather suggest that the cohesive length falls within a bounded range, a result which is consistent with previous studies on elastic-plastic solids by Tvergaard and Hutchinson (1992). The upper bound is defined by the triangular interface law but there seemed to be no well-defined lower bound.

5. Effects of statistical microstructures with triangular interface laws

The DEM models presented so far in this study had perfectly periodic microstructures with no statistical variations. Biological and synthetic bioinspired staggered composites however show significant statistical variations in their microstructure including variations in tablet size and arrangement (Fig. 1). These materials also show variations in their constituent properties that include material heterogeneities within the tablets and the interfaces. We used the DEM models to capture the impact of these statistical variations on toughness. Models were first created following the procedure above to generate an array of initial positions for the center of the tablets. These positions were then perturbed by a random distance that followed a normal distribution centered on zero. The position of the ends of the tablets was then determined, each tablet end being exactly at the midpoint between two adjacent tablet centers. This procedure resulted in arrays of tablets with an average aspect ratio $\overline{\rho}$ and a standard deviation $\Delta\rho$, and to characterize the amount of statistics in the microstructure we used

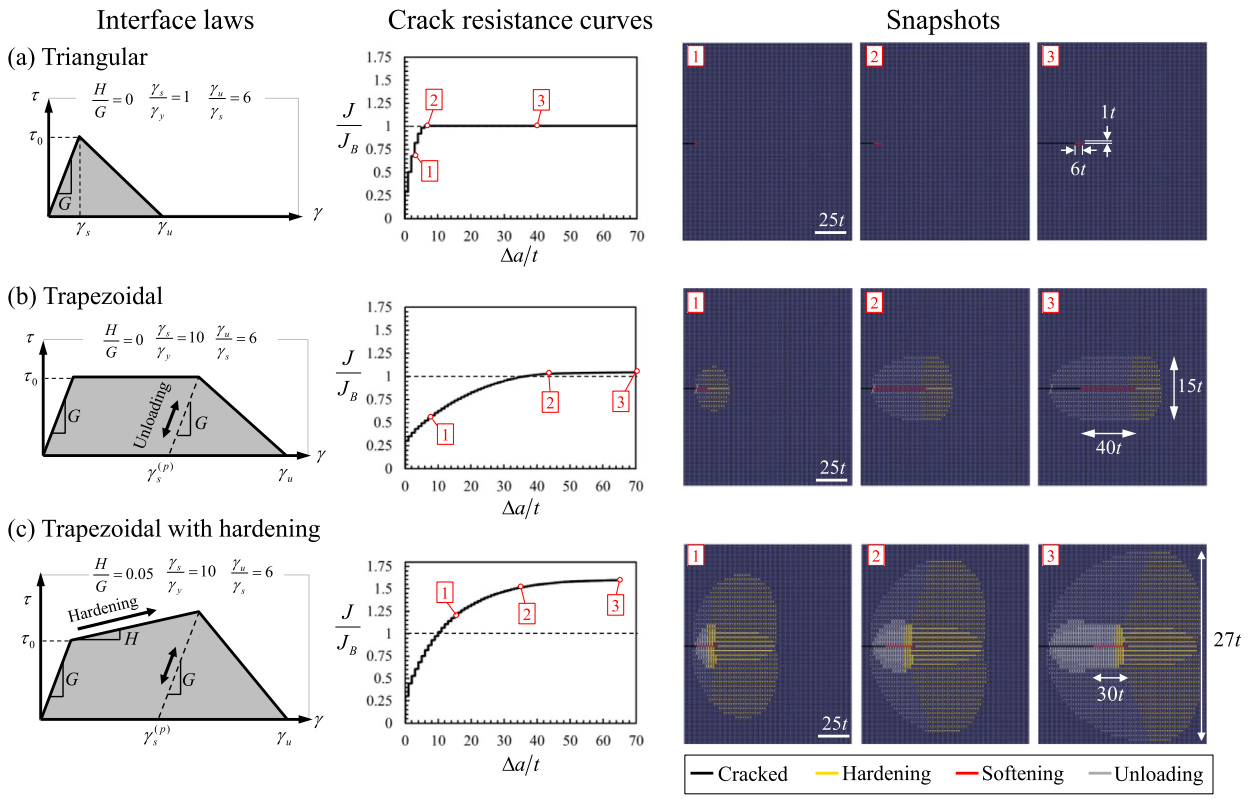

Fig. 6. Three models of columnar nacre where $\kappa = 0.25$ and $\rho = 4$ with different interface laws: (a) triangular, (b) trapezoidal and (c) trapezoidal with hardening. For each case we show the shear stress-strain curve, the crack resistance curve and snapshots that show the development of the process zone development and crack propagation (The snapshots are magnified, the size of the full models is $N_x = 1{,}500$ by $N_y = 300$ tablets.

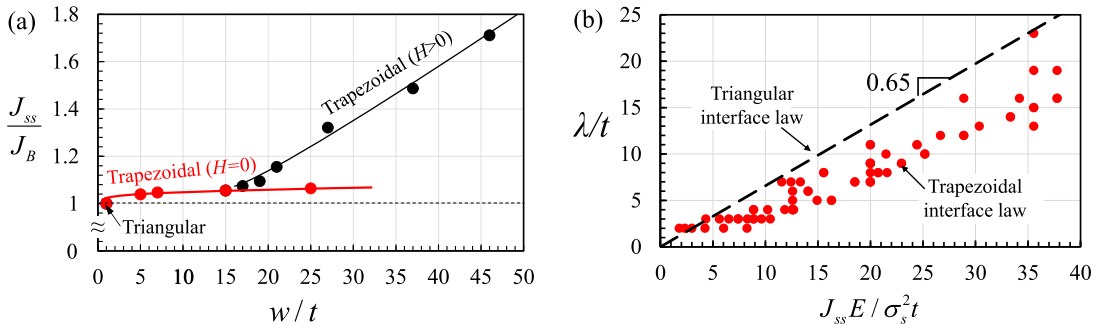

Fig. 7. (a) Effect of the dimensionless process zone width on the dimensionless steady state toughness; (b) Dimensionless cohesive length λ/t as function of $J_{SS}E/\sigma_s^2 t$ with trapezoidal interface laws.

the normalized standard deviation $\Delta\rho/\overline{\rho}$. Using this method, we could generate microstructure with moderate variations ($\Delta\rho/\overline{\rho} < 0.125$), higher variations leading to some tablets with negative length. To explore larger variations ($\Delta\rho/\overline{\rho} > 0.125$), we used a log normal distribution which ensured positive tablet length but which could only be applied to sheet nacre (i.e. only for cases where there is no correlation of position across layers). Further details on the procedure of introducing statistical variations can be found in our previous study (Abid et al., 2018). Fig. 8 shows a sample of three different types of microstructures with different amounts of statistical variations, with the thicker black interfaces representing the pre-crack in the model.

The first set of calculations was performed using a simple triangular interface law (with $\tau_y/G = 0.09$ and $\gamma_u/\gamma_s = 4$) on large DEM fracture models ($N_x = 1{,}000$ by $N_y = 200$ tablets). We considered three cases: $\Delta\rho/\overline{\rho} = 0.0$ (columnar nacre model, no statistical variation, perfectly periodic microstructures), $\Delta\rho/\overline{\rho} = 0.075$ (columnar nacre model, moderate statistical variations) and $\Delta\rho/\overline{\rho} = 0.35$ (sheet nacre model, large statistical variations). Fig. 9 shows the crack path and the corresponding crack resistance curve for each three cases. The first case ($\Delta\rho/\overline{\rho} = 0$) is identical to the case reported in Fig. 3, with a

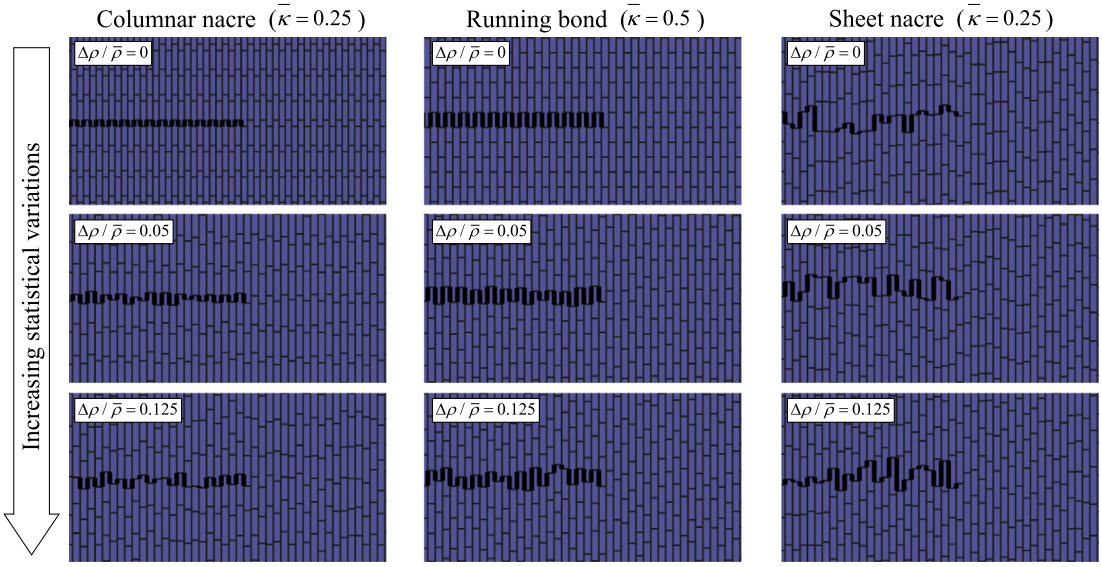

Fig. 8. Close up regions of DEM fracture models with three types of microstructures and three level of statistical variations. The thick black interface represents the pre-crack in the model.

straight crack propagation and a "flat" crack resistance curve. In the second case $\Delta\rho/\bar{\rho} = 0.075$, weak and tough regions are present in the microstructure. If the tougher regions are sufficiently large, the crack is pinned and reinitiating crack growth requires an increase in the applied J. Crack may then propagate again either through the tougher region as shown on snapshot 1 (Fig. 9b), or be deflected as shown on snapshot 2 (Fig. 9b). Once the crack is unpinned and propagates again, the cohesive length from the pinning still overlaps with the cohesive length of the crack and therefore it continues to contribute to crack closure. For this reason, the overall crack resistance only decreases gradually until the next pinning event. There are also cases where the crack is "easily" deflected and channeled by weak regions, in which case no increase of toughness as shown on snapshot 3 (Fig. 9b). This case illustrates that in general, crack deflection in materials should not be systematically associated with an increase in toughness. On the example of Fig. 9b the crack was pinned and unpinned multiple times over the course of the simulation, causing the R-curve to fluctuate whereby the overall the crack resistance increase of about 30% compared to the perfectly period microstructure. Here the fluctuations of the R-curve are not due to plastic unloading occurring at the crack tip, but rather to the pinning events. Similar fluctuating R-curves have been observed experimentally (Davidson and Waas, 2012; De Morais and Pereira, 2007) and computationally (Hossain et al., 2014; Roux et al., 2003). A decrease in the R-curve does not indicate that the J-integral becomes path dependent, as was shown in the works of Hossain, Hsueh (Hossain et al., 2014). In the last case which had the most statistical variations ($\Delta\rho/\bar{\rho} = 0.35$), the crack never propagates straight and is consistently deflected, producing a jagged propagation path (Fig. 9c). The crack experiences more pronounced pinning which almost doubles the crack resistance.

In order to examine a more complete description of how statistics influences the fracture toughness, we performed an exhaustive parameter study by varying $\Delta\rho/\bar{\rho}$ from 0 to 0.125 for columnar and running bond models, and varying $\Delta\rho/\bar{\rho}$ from 0 to 0.7 for sheet nacre models. For each value of $\Delta\rho/\bar{\rho}$, we simulated five realizations of the statistical model with $N_x = 1{,}000$ and $N_y = 200$ tablets. Five realizations per increment was sufficient as the crack was allowed to propagate by a maximum of 200 tablet thicknesses in each model. Therefore, five realizations sampled enough data points (nearly 1000 units of crack growth or 1000J values) to accurately capture the toughness of each type of microstructure considered here. We verified, on models with large statistical variations, that simulating more realizations of the same microstructure did not affect the statistical variations of the measured toughness. There are several ways to extract a single representative toughness measure of a R-curve including ASTM standards, which is only applicable for a "typical" R-curve (Srivastava et al., 2014), corrected beam theory, which is only applicable for double cantilever beam specimens (Blackman et al., 1995; De Morais and Pereira, 2007) and curve fitting, which is good for low fluctuation (Heide-Jørgensen et al., 2018). The majority, on the other hand, used the maximum, average or minimum of the values on the R-curve to define the toughness despite not reaching steady state (Davidson and Waas, 2012; Heide-Jørgensen and Budzik, 2018; Hossain et al., 2014) and that is the approach that we have adopted for this study. Therefore, for each realization we determined the maximum toughness, the minimum toughness, and the average toughness over entire crack resistance curve. We then averaged each of these values over the five realizations. The results (Fig. 10a) show that small amounts of statistical variation increase the toughness in all types of nacre, a phenomenon which is the most pronounced in columnar and sheet nacres. In the case of running bond microstructures the average toughness is consistently lower than the bridging toughness J_B, because this microstructure produces a stairway type of crack growth, a different failure mechanism where crack bridging is not effective

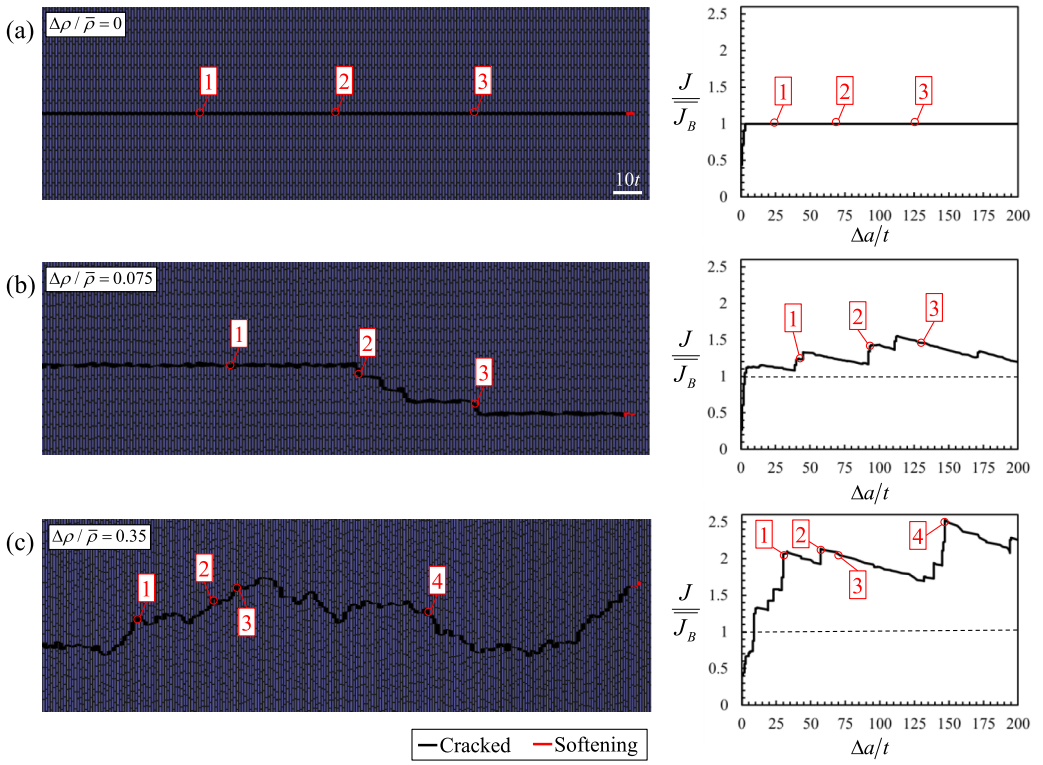

Fig. 9. Effect of statistics for (a) $\Delta\rho/\overline{\rho}=0$ (columnar nacre), (b) $\Delta\rho/\overline{\rho}=0.075$ (columnar nacre) and (c) $\Delta\rho/\overline{\rho}=0.35$ (sheet nacre) with a triangular interface law where $\tau_y/G=0.09$ and $\gamma_u/\gamma_s=4$. The left column shows a close up of the model, and the right column shows the corresponding crack resistance curve. The snapshots were cropped to show only a part of the crack. The size of the full model was $N_x=1000$ by $N_y=200$ tablets.

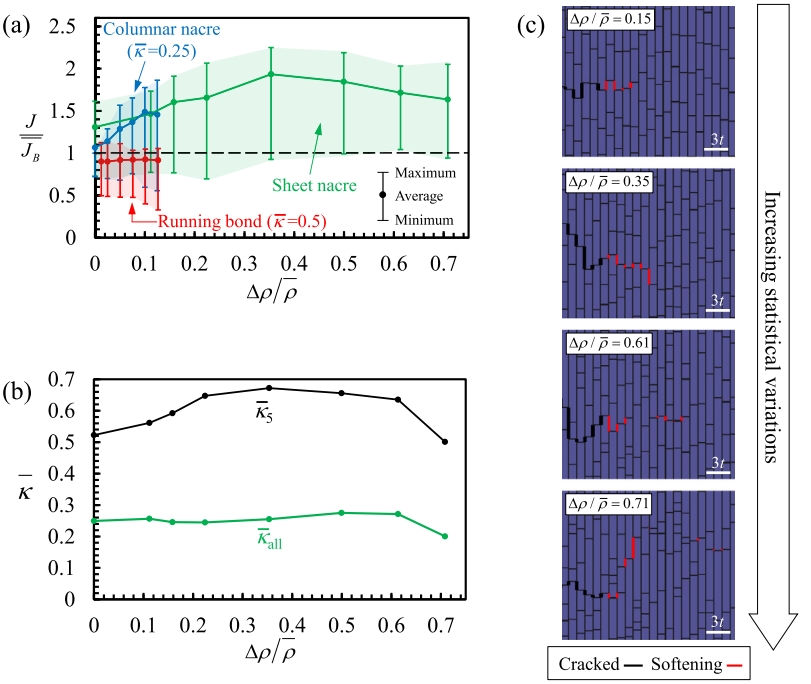

Fig. 10. Effect of statistical variations on (a) the normalized toughness and (b) the average normalized interface length ($\overline{\kappa}$) of all the interfaces together and the average of the five toughest interfaces collected along cracks paths in sheet nacre. (c) Typical snapshots of crack propagating through sheet nacre models with four levels of statistical variations. Here, a triangular interface law was used with $\tau_y/G=0.09$ and $\gamma_u/\gamma_s=4$. Each point on the curve is an average of 5 realization.

(Rabiei et al., 2010). The sheet nacre microstructures could be modeled with larger statistical variations, with a toughness that decreases when $\Delta\rho/\overline{\rho} > 0.35$. This initial increase and then decrease of toughness with statistical variations can be explained by collecting the lengths of the individual fractured interfaces (normalized by $\overline{\rho}t$). The average length of these interfaces ($\overline{\kappa}_{all}$), shown on Fig. 10b, fluctuates around $\overline{\kappa} = 0.25$ with no apparent effect of statistics. The average of the five longest interfaces travelled by the crack ($\overline{\kappa}_5$) captured the pinning efficacy of the toughest obstacles encountered during crack propagation. Fig. 10b shows how $\overline{\kappa}_5$ initially increases when statistics is increased, but decreases for $\Delta\rho/\overline{\rho} > 0.35$, which indicates that the pinning sites explored by the crack are weaker for higher statistics. Fig. 10c shows typical snapshots of crack propagating through sheet nacre models with four levels of statistical variations. For small statistical variations the cohesive zone is compact and concentrated at the crack tip. As statistical variations increase, daughter cracks form ahead of the main crack, at distances what can be several tablets and which tend to be greater in models with larger randomness. Eventually these cracks coalesce to form the main crack, and the phenomenon repeats further into the material. This observation reveals an interesting mechanism which explains the variations of overall toughness with statistical variations. Increasing statistical variations generally means that the toughest regions in the model increase in toughness, and the weakest regions become weaker. At moderate statistical variations the crack follows the weakest path presented directly ahead of the tip, which sometimes takes it into a tougher region, where it gets pinned. Moderate increases in statistics generate tougher region, more intense pinning and therefore increased overall toughness. Large statistical variations generate even tougher regions, but also very weak regions. In that second regime, the weaker regions are so weak that they can be "activated" by the stresses around the crack at some distance of the main cohesive zone, forming daughter cracks as seen on Fig. 10c. Importantly, the crack eventually coalesces through these weaker regions and the phenomenon repeats further into the material. The ability of the crack to "probe" further into the material means that it can find the weakest path more effectively, that it can avoid large obstacles (hence the decrease in $\overline{\kappa}_5$ shown on Fig. 10b), and that as a result the overall toughness will be decreased. Statistical variations are therefore beneficial only if the cohesive zone remains compact and when the crack is more likely to meet strong pinning regions. Higher statistical variations are more likely to activate weaker paths within larger regions around the main crack, so that tougher regions are more likely to be avoided.

6. Effects of statistical microstructures with trapezoidal interface law

In this section we examine the effect of statistics with a trapezoidal interface law with and without strain hardening, so that the process zone is no longer confined to a narrow region. The interface law parameters were fixed at $\tau_y/G = 0.09$, $\gamma_u/\gamma_s = 4$, $\gamma_s/\gamma_y = 10$ and $H/G = 0.05$. For each level of statistics ($\Delta\rho/\overline{\rho} = 0$, 0.025, 0.05, 0.075, 0.1, 0.125), five realizations were simulated for each type of microstructures (columnar nacre, running bond nacre and sheet nacre). Crack propagation was generally stable at the beginning of the simulation, but most models ceased to converge before the crack could completely fracture the model. Fig. 11 shows the contours of the last loading step for the three types of microstructures with three levels of statistics ($\Delta\rho/\overline{\rho} = 0$, 0.05, 0.125) with a trapezoidal with hardening interface law. For the columnar nacre with no statistics ($\Delta\rho/\overline{\rho} = 0$), the crack propagation was perfectly straight, and the process zone was dense and symmetric (this case is identical to the case shown on Fig. 6c). In the running bond case with no statistics ($\Delta\rho/\overline{\rho} = 0$), a triangular inelastic region initially formed ahead of the notch. The crack then propagated in a "staircase" manner, which can occur when the overlap between the tablets is relatively uniform (this failure mode is generated by the shear stress field ahead of the crack, as described in details in (Rabiei et al., 2010)). In the case of sheet nacre the crack deflected slightly, and the process zone was more diffuse with a less well defined shape. When a small amount of statistics is added on the three types of microstructure, crack deflection occurred more frequently. Generally, the process zone increased in size because high stresses associated with the crack can "activate" weaker region located further from the crack lines, so that the high stresses generated by the crack tip have can reach further within the volume of the material. The resulting process zone was however more sparse and heterogeneous compared to the cases with no statistics, and that the density of energy absorbed in the wake was not as high as for the perfect microstructures. The process zone of the running bond case when $\Delta\rho/\overline{\rho} = 0.05$ is a dense "v-shaped" which was also observed by Pro, Lim (Pro et al., 2015). Interestingly, for the cases where the statistical variation was the highest ($\Delta\rho/\overline{\rho} = 0.125$) it was not possible to distinguish between the microstructure types, because the large statistical disturbances imposed on each of the three types of microstructure completely obscured their original, distinct characteristics. For this reason, the failure mechanisms were similar across all three types of microstructure (Fig. 11). The process zone had no well-defined shape and only consisted of widespread sparse and disconnected yielded interfaces. Fig. 12 shows the corresponding crack resistance curves for these models. For each level of statistics, five realizations were evaluated. Generally the crack resistance curves were rising with crack advance, to levels which are significantly higher than the toughness from bridging only. As expected the spread in the results increased as statistical variations were increased. Generally toughness increased when a small amount of statistic was introduced, but decreased for the highest levels of statistics.

For each model we computed the minimum, maximum and average toughness from the crack resistance curve, which is the most appropriate method for relatively large fluctuating *R*-curves (Davidson and Waas, 2012). A summary of these results is shown in Fig. 13, where the average of the five models was again taken for each level of statistics. The results show that the toughness for hardening interfaces ($H/G = 0.05$) is generally higher than when no hardening is used ($H/G = 0$), because interface hardening produces a larger and denser process zone and therefore higher energy dissipation overall. In general, the overall toughness increases as statistics is introduced up to a peak value in the range $\Delta\rho/\overline{\rho} = 0.05 - 0.075$.

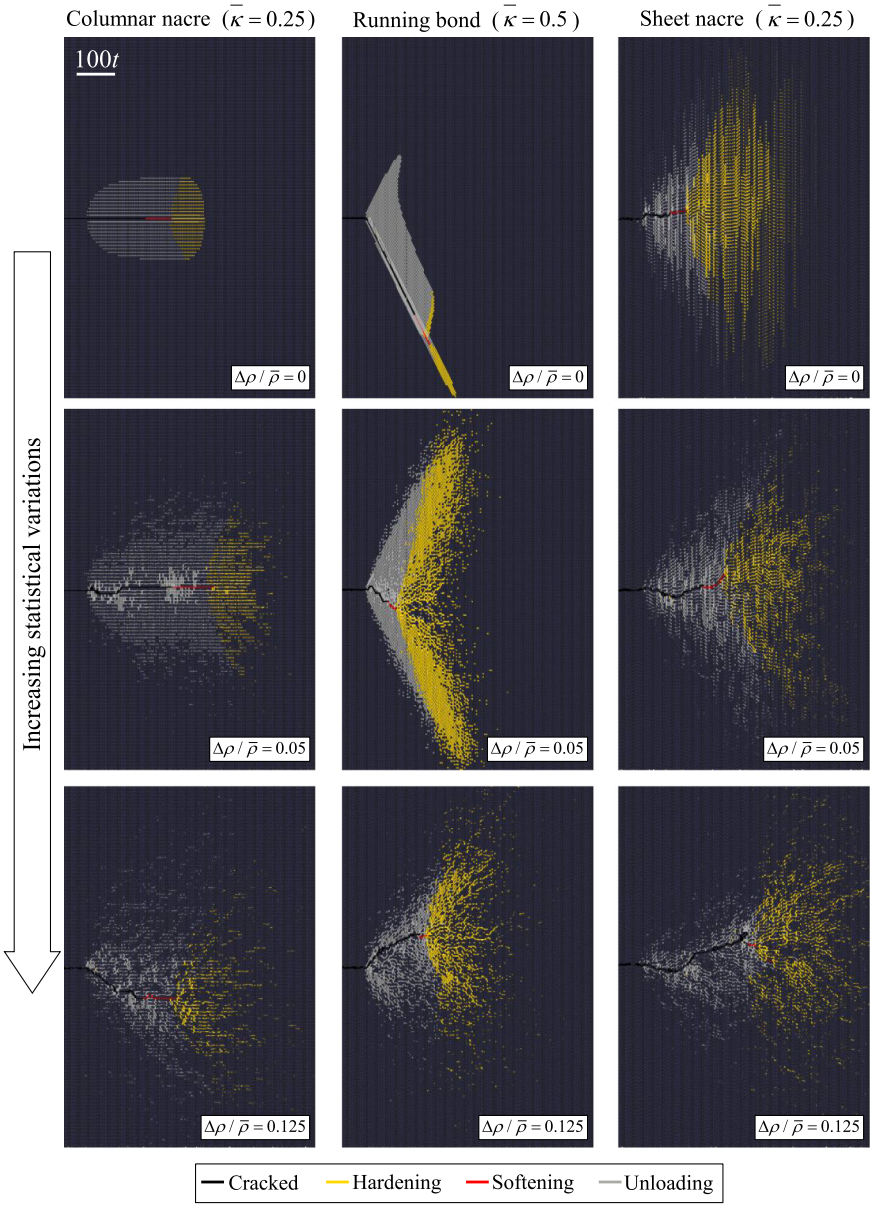

Fig. 11. Snapshots of DEM simulations for columnar nacre (left column), running bond (middle column), and sheet nacre (right column) at three levels of statistical variations. The simulation snapshots are cropped to only show the crack propagation and the process zone. (Full model was $N_x = 1{,}500$ by $N_y = 300$ tablets) .

Larger statistical variations beyond these values leading to an overall decrease in toughness. We attributed this behavior to a competition between process zone size, density, and weakest path for the crack. Moderate amounts of statistical variations promote toughness because of crack pinning, and increased process zone size. However when the statistic variation become too large, the crack finds an easy path through the weakest regions in the model, and the process zone become less dense, resulting in a decrease in toughness. Again, all three microstructures produced nearly the same amount of toughness when large statistical variation is present ($\Delta\rho/\bar{\rho} = 0.125$) which shows again that the presence of large statistics variations diminishes the original characteristics of each microstructure. We acknowledge that there are few *R*-curves that do not reach steady state in Fig. 12 due to convergence issues. However, sampling these models out would create an unwanted bias. These *R*-curves stopped due to extreme pinning and as result the *J* value would decrease if the crack were to progress. For the models that did converge, we simulated larger crack growth and the *R*-curve seems to fluctuate in a bounded region and the mean *J* value remained unchanged. Despite the unsteady *R*-curves, one can visually see on Fig. 12 that there is an optimum value of statistics and that large statistics reduces the toughness.

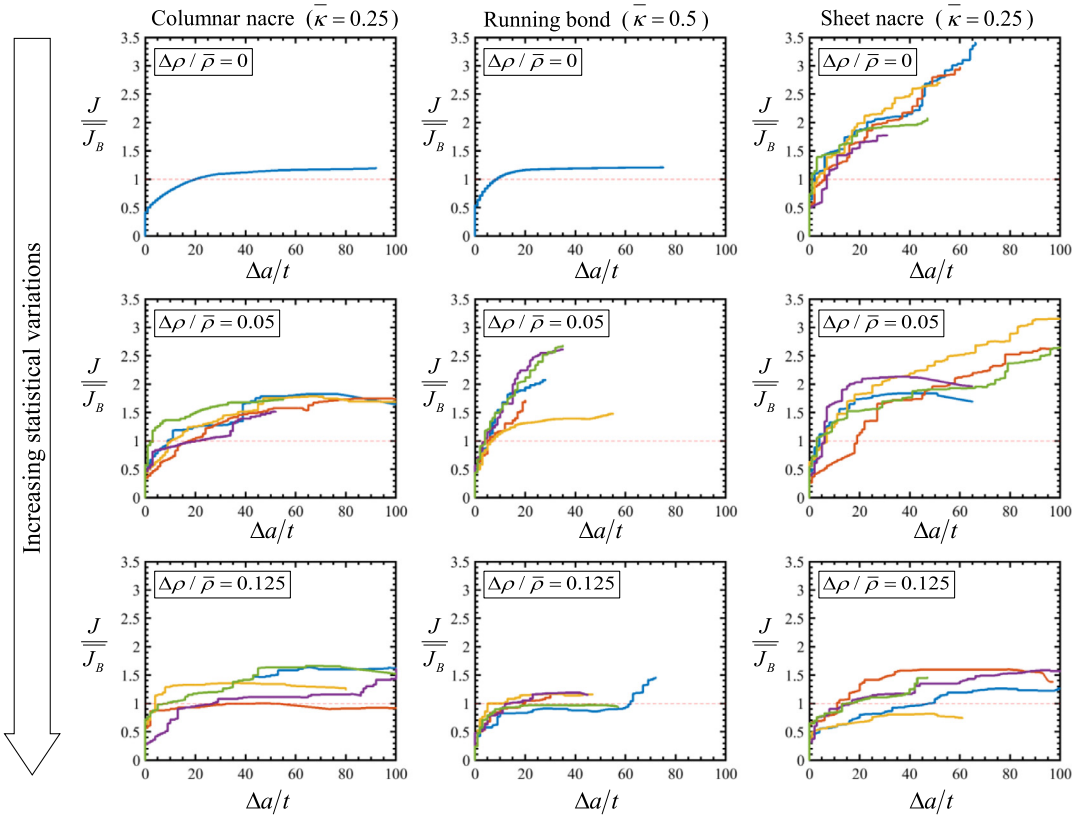

Fig. 12. Crack resistance curves for columnar nacre (left column), running bond (middle column), and sheet nacre (right column) at three levels of statistical variations. Each graph shows five realizations of the same statistics.

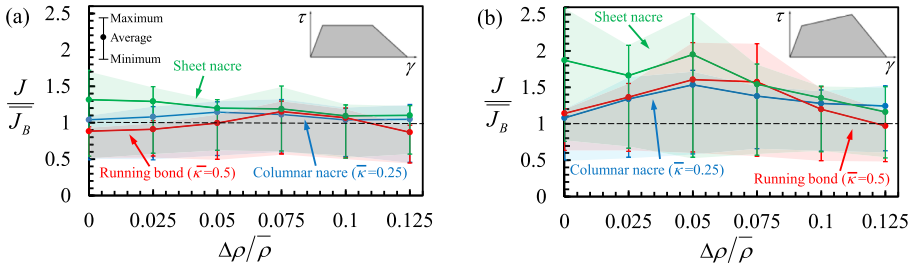

Fig. 13. Effect of statistical variations on the dimensionless toughness for columnar, running bond, and sheet nacre with (a) trapezoidal, no hardening and (b) trapezoidal with hardening interface law where $\tau_y/G = 0.09$, $\gamma_u/\gamma_s = 4$, $\gamma_s/\gamma_y = 10$ and $H/G = 0.05$.

A recent study by Pro, Lim (Pro et al., 2015) showed that initiation toughness decreases substantially with statistical variations for running bond nacre with trapezoidal interface law. In our case, the initiation toughness scales with the minimum toughness reported in Fig. 13 and we observed that the initiation toughness slightly increased due to statistics but decreased beyond the optimum level of statistics. The difference in both the studies could arise from the different solvers used and the assumptions regarding horizontal interfaces, transverse sliding and rotation of tablets, and interface laws.

Finally, Fig. 14 shows a comparison between the micromechanics of fracture captured with our DEM model and experimental observations on the fracture of columnar and sheet nacre (Rabiei et al., 2010). This comparison is meant to be qualitative as the experiments may consist of different tablet aspect ratio, statistics, interface properties, etc. Our models can capture the different types of crack paths possible (relatively straight for columnar nacre, deflected branches for sheet nacre) and the shape of the process zone (transition region at the edges, compact in columnar nacre and more sparse in sheet nacre (Keten et al., 2010)).

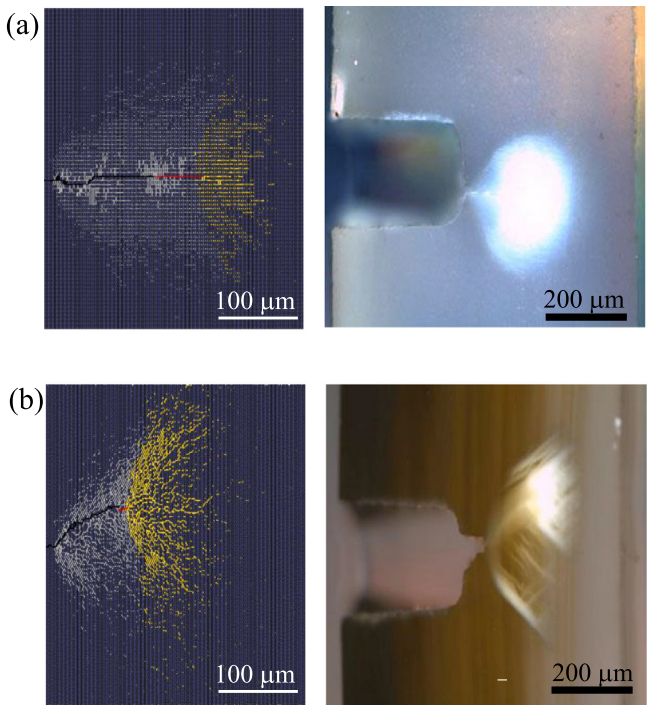

Fig. 14. Side by side comparisons between our DEM results and experimental observation on the fracture of (a) a columnar nacre (Top shell) and (b) a sheet nacre (Pearl oyster) (adapted from Rabiei, Bekah (Rabiei et al., 2010)).

7. Summary and conclusion

The staggered architecture is found in high-performance structural biological materials such as nacre, bone, tooth enamel and spider silk. This architecture produces unique combinations of stiffness, strength and toughness, and for this reason it is often used as model for developing modern composite materials. In this study we used discrete element modeling to explore the fracture mechanics of nacre-like staggered materials, with the main conclusions summarized below:

1 The discrete element models is a powerful, computationally efficient approach that can capture the fracture mechanics of large volumes of nacre-like materials. The computational cost of running discrete element models is a fraction of that of other numerical methods such as finite elements. The predicted fracture modes and process zone shapes are qualitatively consistent with experimental observations on natural nacre. In this study we ran a total of about 180 DEM simulations of large (1500×300 tablets) fracture models. For a given microstructure we evaluated five realizations, which was sufficient to produce reliable statistics for the overall toughness because for each model a large volume of material is interrogated through crack propagation.
2 The fracture models presented here capture the fracture of nacre-like materials: crack deflection, crack bridging, the formation of wide process zone of different size and shapes that depend on the interface and architecture of the material, as well as transient and steady-state crack propagation regimes while relaxing some of the assumptions of the previous models regarding process zone, wake of damage and interface properties. The full crack resistance curve can be determined as function of microstructure and interface properties. The models also capture classical scaling rules in fracture mechanics.
3 When the material is stretched along the direction of the tablets, fracture is governed by the axial displacements of the tablets and their associated interfacial shear stresses. Despite the multiaxial characteristics of the stresses ahead of the crack tip, the transverse displacements and rotations of the individual tablets have a negligible effect on fracture mechanics and on overall fracture toughness.
4 Statistical variations in the microstructure create tougher and weaker regions within the material. Moderate statistical variations generate obstacles which pin propagating cracks, increasing overall toughness, provided that the cohesive zone remains compact. For higher statistical variations the weaker regions are so weak that they can be activated far from the main crack. It then becomes easier for the crack to “probe” larger volumes of materials to find weaker paths. Volumetric process zones are wider, but sparser and they do not dissipate as much energy. These combined effects lead to decreased overall toughness for large statistical variations.
5 In general, crack deflection occurred when it was more advantageous for the crack to deviate and reach weaker regions. Accordingly we observed more crack deflection for models with larger statistical variations, since they contained a larger

number of weaker regions. In our models we observed that crack deflection was simply a mean for the crack to follow the weakest path within the material, with no increase in toughness. In general crack deflection in nacre-like materials is not necessarily associated with an increase in overall toughness.

These findings, together with our previous report that focused on uniaxial deformations (Abid et al., 2018), provide strong evidence that large statistical variations are detrimental to the performance of nacre-like staggered composites. The stagger, size and interfaces of inclusions in these materials should be as uniform as possible to maximize strength, toughness, deformability and energy absorption. Staggered composites in nature can indeed display remarkable periodicities and regularities. For example fibers of collagen type I, which serve as the building blocks for bone, tendon or skin, are made of collagen molecules with a uniform length of 300 nm. The molecules assemble into fibrils by forming highly aligned staggered architectures with a highly uniform overlap length of 67 nm (Fratzl et al., 1998). Individual collagen fibrils are among the strongest and toughest natural fibers (Puxkandl et al., 2002; Shen et al., 2008). Collagen fibrils bundle into fibers, which can for example serve as the primary building blocks of tendons, which are virtually impossible to fracture (Ker, 2007). Natural nacre is another example of a staggered composite with a highly uniform microstructure. The relative statistical variation ($\Delta\rho/\overline{\rho}$) for nacre is about 0.4-0.6 for columnar nacre and 0.5-0.6 for sheet nacre Rabiei, Bekah (Rabiei et al., 2010). These variations are on the higher end of what we explored in this report, but they are much lower than what is observed in synthetic nacres. Fabrication methods such as self-assembly (Bonderer et al., 2008; Valashani et al., 2015), freeze casting (Deville et al., 2006), filtration (Liu et al., 2011), sedimentation (Behr et al., 2015), doctor blading (Mirkhalaf and Barthelat, 2016) or controlled mineralization (Mao et al., 2016) cannot duplicate to this day the regularity of natural nacre at the microscale. Only fabrication methods at larger length scales (manual assembly (Barthelat and Zhu, 2011), 3D printing (Espinosa et al., 2011) or laser engraving (Chintapalli et al., 2014; Valashani and Barthelat, 2015)) can produce highly regular materials which can duplicate the mechanisms of deformations and fracture of natural nacre.

The general findings reported here can possibly be integrated into existing design guidelines (Barthelat, 2014; Begley et al., 2012; Gao, 2006) to further increase the performance of bio-inspired composites at the design stage. Finally, the DEM method described here and applied to large models with statistical variations abstracts the materials as a network of non-linear springs that can deform and fracture. This type of representation can also be used to capture the fracture of other types of composite materials, and also of ceramics and metals where the size of the microstructure is in the order of the size of the cohesive length. The DEM fracture models presented here therefore suggest that, just like in nacre-like materials, the toughness of ceramics and metals decreases with increased statistical variations in their microstructure.

Acknowledgments

This work was supported by a Strategic Grant (STPGP 479137 – 15) from the Natural Sciences and Engineering Research Council of Canada and by a Team Grant (191270) from the Fonds de Recherche du Québec – Nature et Technologies. N.A. was partially supported by a McGill Engineering Doctoral Award.

References

Abid, N., Mirkhalaf, M., Barthelat, F., 2018. Discrete-element modeling of nacre-like materials: Effects of random microstructures on strain localization and mechanical performance. J. Mech. Phys. Solids 112, 385–402.
Anup, S., 2015. Influence of initial flaws on the mechanical properties of nacre. J. Mech. Behav. Biomed. Mater. 46, 168–175.
Askarinejad, S., Rahbar, N., 2015. Toughening mechanisms in bioinspired multilayered materials. J. Royal Soc. Interface 12 (102), 20140855. doi:10.1098/rsif.2014.0855.
Bai, H., et al., 2016. Bioinspired hydroxyapatite/poly (methyl methacrylate) composite with a nacre-mimetic architecture by a bidirectional freezing method. Adv. Mater. 28 (1), 50–56.
Barenblatt, G.I., 1959. The formation of equilibrium cracks during brittle fracture. General ideas and hypotheses. Axially-symmetric cracks. J. Appl. Math. Mech. 23 (3), 622–636.
Barthelat, F., et al., 2007. On the mechanics of mother-of-pearl: A key feature in the material hierarchical structure. J. Mech. Phys. Solids 55 (2), 306–337.
Barthelat, F., 2010. Nacre from mollusk shells: a model for high-performance structural materials. Bioinspiration Biomim. 5 (3), 035001.
Barthelat, F., 2014. Designing nacre-like materials for simultaneous stiffness, strength and toughness: Optimum materials, composition, microstructure and size. J. Mech. Phys. Solids 73, 22–37.
Barthelat, F., 2015. Architectured materials in engineering and biology: fabrication, structure, mechanics and performance. Int. Mater. Rev. 60 (8), 413–430.
Barthelat, F., Espinosa, H.D., 2007. An experimental investigation of deformation and fracture of Nacre–mother of pearl. Exp. Mech. 47 (3), 311–324.
Barthelat, F., Mirkhalaf, M., 2013. The quest for stiff, strong and tough hybrid materials: an exhaustive exploration. J. Royal Soc. Interface 10 (89), 20130711.
Barthelat, F., Rabiei, R., 2011. Toughness amplification in natural composites. J. Mech. Phys. Solids 59 (4), 829–840.
Barthelat, F., Yin, Z., Buehler, M.J., 2016. Structure and mechanics of interfaces in biological materials. Nat. Rev. Mater. 1, 16007.
Barthelat, F., Zhu, D., 2011. A novel biomimetic material duplicating the structure and mechanics of natural nacre. J. Mater. Res. 26 (10), 1203–1215.
Begley, M.R., et al., 2012. Micromechanical models to guide the development of synthetic 'brick and mortar'composites. J. Mech. Phys. Solids 60 (8), 1545–1560.
Behr, S., et al., 2015. Large-scale parallel alignment of platelet-shaped particles through gravitational sedimentation. Sci. Rep. 5.
Blackman, B., et al., 1995. The failure of fibre composites and adhesively bonded fibre composites under high rates of test. J.Mater. Sci. 30 (23), 5885–5900.
Bonderer, L.J., Studart, A.R., Gauckler, L.J., 2008. Bioinspired design and assembly of platelet reinforced polymer films. Science 319 (5866), 1069–1073.
Chalkley, P., Chiu, W., 1993. An improved method for testing the shear stress/strain behaviour of adhesives. Int. J. Adhes. Adhes. 13 (4), 237–242.
Chandler, M.Q., Cheng, J.-R.C., 2018. Discrete element modeling of microstructure of nacre. Comput. Part. Mech. 5 (2), 191–201.
Chintapalli, R.K., et al., 2014. Strain rate hardening: a hidden but critical mechanism for biological composites? Acta biomaterialia 10 (12), 5064–5073.
Davidson, P., Waas, A.M., 2012. Non-smooth mode I fracture of fibre-reinforced composites: an experimental, numerical and analytical study. Phil. Trans. R. Soc. A 370 (1965), 1942–1965.
De Morais, A., Pereira, A., 2007. Application of the effective crack method to mode I and mode II interlaminar fracture of carbon/epoxy unidirectional laminates. Composites Part A Appl. Sci. Manuf. 38 (3), 785–794.

Deville, S., et al., 2006. Freezing as a path to build complex composites. Science 311 (5760), 515–518.
Dugdale, D.S., 1960. Yielding of steel sheets containing slits. J. Mech. Phys. Solids 8 (2), 100–104.
Espinosa, H.D., et al., 2011. Tablet-level origin of toughening in abalone shells and translation to synthetic composite materials. Nat.Commun. 2.
Evans, A.G., et al., 1986. Mechanisms of toughening in rubber toughened polymers. Acta Metallurgica 34 (1), 79–87.
Fratzl, P., et al., 1998. Fibrillar structure and mechanical properties of collagen. J. Struct. Biology 122 (1-2), 119–122.
Gao, H.J., 2006. Application of fracture mechanics concepts to hierarchical biomechanics of bone and bone-like materials. Int. J. Fract. 138 (1-4), 101–137.
Guo, X., Gao, H., 2006. Bio-inspired Material Design and Optimization. Springer.
Gupta, H.S., et al., 2006. Cooperative deformation of mineral and collagen in bone at the nanoscale. Proc. Natl . Acad. Sciences 103 (47), 17741–17746.
Heide-Jørgensen, S., Budzik, M.K., 2018. Effects of bondline discontinuity during growth of interface cracks including stability and kinetic considerations. J. Mech. Phys. Solids 117, 1–21.
Heide-Jørgensen, S., de Freitas, S.T., Budzik, M.K., 2018. On the fracture behaviour of CFRP bonded joints under mode I loading: Effect of supporting carrier and interface contamination. Composites Sci. Technol. 160, 97–110.
Hillerborg, A., Modéer, M., Petersson, P.E., 1976. Analysis of crack formation and crack growth in concrete by means of fracture mechanics and finite elements. Cement Concrete Res. 6 (6), 773–781.
Hossain, M., et al., 2014. Effective toughness of heterogeneous media. J. Mech. Phys. Solids 71, 15–32.
Katti, D.R., Katti, K.S., 2001. Modeling microarchitecture and mechanical behavior of nacre using 3D finite element techniques. Part 1. Elastic properties. J. Mater. Sci. 36, 1411–1417.
Ker, R.F., 2007. Mechanics of tendon, from an engineering perspective. Int. J. Fatigue 29 (6), 1001–1009.
Keten, S., et al., 2010. Nanoconfinement controls stiffness, strength and mechanical toughness of [beta]-sheet crystals in silk. Nat. Mater. 9 (4), 359–367.
Kolednik, O., Schöngrundner, R., Fischer, F., 2014. A new view on J-integrals in elastic–plastic materials. Int. J. Fract. 187 (1), 77–107.
Lawn, B., 1993. Fracture of Brittle Solids. Cambridge university press.
Liu, A.D., et al., 2011. Clay nanopaper with tough cellulose nanofiber matrix for fire retardancy and gas barrier functions. Biomacromolecules 12 (3), 633–641.
Mao, L.B., et al., 2016. Synthetic nacre by predesigned matrix-directed mineralization. Science 354 (6308), 107–110.
Mathews, J.H., Fink, K.D., 2004. Numerical Methods Using MATLAB, 4. Pearson, London, UK.
Mayer, G., 2005. Rigid biological systems as models for synthetic composites. Science 310 (5751), 1144–1147.
Mirkhalaf, M., Barthelat, F., 2016. Nacre-like materials using a simple doctor blading technique: Fabrication, testing and modeling. J. Mech. Behav. Biomed.l Mater. 56, 23–33.
Munch, E., et al., 2008. Tough, bio-inspired hybrid materials. Science 322 (5907), 1516–1520.
Needleman, A., Tvergaard, V., 1991. A numerical study of void distribution effects on dynamic, ductile crack growth. Eng. Fract. Mech. 38 (2), 157–173.
Nguyen, V.-D., et al., 2012. Imposing periodic boundary condition on arbitrary meshes by polynomial interpolation. Comput. Mater. Sci. 55, 390–406.
Niebel, T.P., et al., 2016. Role of the polymer phase in the mechanics of nacre-like composites. J. Mech. Phys. Solids 96, 133–146.
Nishikawa, S., 1992. Correlation of the arrangement pattern of enamel rods and secretory ameloblasts in pig and monkey teeth: a possible role of the terminal webs in ameloblast movement during secretion. Anat. Rec. 232 (4), 466–478.
Press, W.H., et al., 2007. Numerical Recipes 3rd Edition: The Art of Scientific Computing. Cambridge University Press, p. 1256.
Pro, J.W., et al., 2015. GPU-based simulations of fracture in idealized brick and mortar composites. J. Mech. Phys. Solids 80, 68–85.
Pro, J.W., et al., 2015. The impact of stochastic microstructures on the macroscopic fracture properties of brick and mortar composites. Extreme Mech. Lett. 5, 1–9.
Puxkandl, R., et al., 2002. Viscoelastic properties of collagen: synchrotron radiation investigations and structural model. Philos. Trans. Royal Soc. Lond. B-Biol. Sci. 357 (1418), 191–197.
Rabiei, R., Bekah, S., Barthelat, F., 2010. Failure mode transition in nacre and bone-like materials. Acta Biomaterialia 6 (10), 4081–4089.
Rice, J., 1979. The Mechanics of Earthquake Rupture. Division of Engineering, Brown University.
Rice, J., Rosengren, G.F., 1968. Plane strain deformation near a crack tip in a power-law hardening material. J. Mech. Phys. Solids 16 (1), 1–12.
Rice, J.R., 1968. A path independent integral and the approximate analysis of strain concentration by notches and cracks. J. Appl. Mech. 35 (2), 379–386.
Roux, S., Vandembroucq, D., Hild, F., 2003. Effective toughness of heterogeneous brittle materials. Eur. J. Mech. A/Solids 22 (5), 743–749.
Shen, Z.L., et al., 2008. Stress-strain experiments on individual collagen fibrils. Biophys. J. 95 (8), 3956–3963.
Simha, N., et al., 2008. J-integral and crack driving force in elastic–plastic materials. J. Mech. Phys. Solids 56 (9), 2876–2895.
Smith, B.L., et al., 1999. Molecular mechanistic origin of the toughness of natural adhesives, fibres and composites. Nature 399 (6738), 761–763.
Srivastava, A., et al., 2014. Effect of inclusion density on ductile fracture toughness and roughness. J. Mech. Phys. Solids 63, 62–79.
Tada, H., Paris, P.C., Irwin, G.R., 1973. The Stress Analysis of Cracks. Handbook. Del Research Corporation.
Tvergaard, V., Hutchinson, J.W., 1992. The relation between crack growth resistance and fracture process parameters in elastic-plastic solids. J. Mech. Phys. Solids 40 (6), 1377–1397.
Valashani, S.M.M., Barrett, C.J., Barthelat, F., 2015. Self-assembly of microscopic tablets within polymeric thin films: a possible pathway towards new hybrid materials. RSC Adv. 5 (7), 4780–4787.
Valashani, S.M.M., Barthelat, F., 2015. A laser-engraved glass duplicating the structure, mechanics and performance of natural nacre. Bioinspiration Biom. 10 (2).
Wegst, U.G., et al., 2015. Bioinspired structural materials. Nat. Mater. 14 (1), 23–36.